Highly Strained Compliant Optical Metamaterials with Large Frequency Tunability

Imogen M. Pryce,[†,§] Koray Aydin,[†,§] Yousif A. Kelaita,[†] Ryan M. Briggs,[†] and Harry A. Atwater*,[†,‡]

[†]Thomas J. Watson Laboratories of Applied Physics and [‡]Kavli Nanoscience Institute, California Institute of Technology, Pasadena, California 91125

ABSTRACT Metamaterial designs are typically limited to operation over a narrow bandwidth dictated by the resonant line width. Here we report a compliant metamaterial with tunability of $\Delta\lambda \sim 400$ nm, greater than the resonant line width at optical frequencies, using high-strain mechanical deformation of an elastomeric substrate to controllably modify the distance between the resonant elements. Using this compliant platform, we demonstrate dynamic surface-enhanced infrared absorption by tuning the metamaterial resonant frequency through a CH stretch vibrational mode, enhancing the reflection signal by a factor of 180. Manipulation of resonator components is also used to tune and modulate the Fano resonance of a coupled system.

KEYWORDS Metamaterials, polymers, plasmonic sensing

Metamaterials are artificially engineered composites that can exhibit optical responses unattainable in their component materials.[1−4] The optical response of a metamaterial can be engineered by manipulation of the size, pattern, and composition of its subwavelength unit cells. This response, however, is usually fixed at the time of fabrication yielding materials that are essentially "passive" and operate over a limited bandwidth. The response of otherwise passive metamaterials can be rendered active by integrating dynamic components into the design. Active metamaterials, which seek to tune the resonant frequency range via control of the active medium, represent a new class of designs. To date, amplitude modulation of optical metamaterials, which affects the intensity of the response at the resonant wavelength, has been achieved via electrical carrier injection in semiconductor substrates[5] and mechanical reorientation of resonant elements using microelectromechanical systems.[6] Frequency tunability has been demonstrated by changing the dielectric environment of the resonator with phase-transition materials,[7,8] liquid crystals,[9] and optical pumping of the substrate.[10] Here we take a different approach and exploit the elasticity of a compliant substrate to tune the resonant frequency of a metamaterial in the near-infrared by changing the distances and thus the coupling strength between pairs of resonator elements.

Stretchable electronics have recently garnered increasing interest,[11] and though mechanical deformation of elasto-meric substrates has been used to induce spectral shifts in the resonance of nanophotonic structures such as nanoparticle dimer extinction[12] and gratings,[13] the reported tunability range was limited. Our results represent the first demonstration of broad tunability of metamaterials via the elastic and plastic deformation of compliant substrates and, surprisingly, the nanoscale resonator arrays can be subjected to tensile strains as high as $50 \pm 1\%$ without delamination or distortion of the metallic elements. Although flexible metamaterials have been fabricated to operate at microwave[14] and terahertz[15,16] frequencies, compliant tuning of metamaterials has not previously been shown. We also demonstrate tunable Fano resonances[17−20] utilizing the mechanical deformation of compliant dolmen-type resonator arrays.

The metamaterial structures investigated are planar, coupled split-ring resonator (SRR) arrays in which the resonant frequency depends on the geometry of the SRR and the complex refractive index of the metamaterial substrate. At optical frequencies, U-shaped SRRs have been extensively studied[21,22] and can be modeled as electrical LC resonators with a resonant frequency of $\omega_0 \sim (LC)^{-1/2}$, where the effective capacitance C depends on the gap size, and the inductance L is proportional to the total effective length of each SRR. This resonant frequency can be altered by changing the geometry of the SRR or by introducing a coupling element, such as a nanowire. This introduces an additional parameter, the coupling constant, that provides further control over the resonant wavelength of metamaterial structures. The coupling constant depends on the distance between the resonator pairs, and we have previously reported that for passive structures changing the coupling distance results in a significant shift in the resonant frequency re-

* To whom correspondence should be addressed. E-mail: haa@caltech.edu.

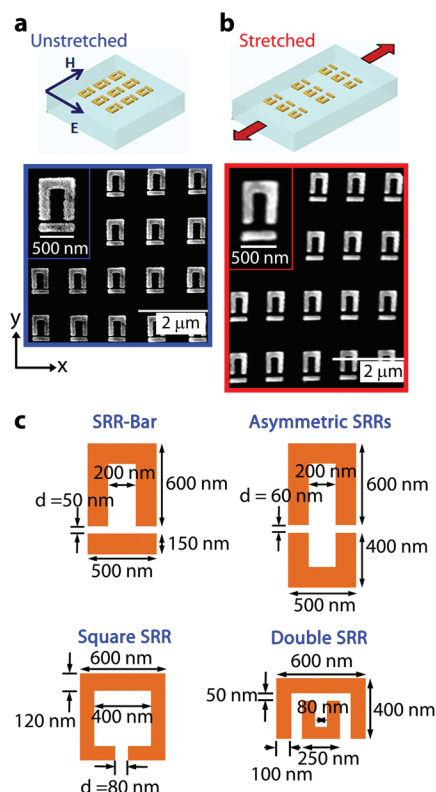§ These authors contributed equally to this work.

FIGURE 1. (a) The top panel is a schematic of the substrate prior to stretching with Au split ring resonators attached. The polarization of the incident electromagnetic radiation is also indicated. The bottom panel shows environmental scanning electron microscope (ESEM) images of a unit cell and representative array prior to stretching. (b) The top panel shows a schematic of a stretched array. The bottom panel is ESEM images corresponding to 50% strain of the array in (a). (c) Schematics of each unit cell structure studied with dimensions: SRR-bar, asymmetric SRRs, square SRR, and double SRR structures.

sponse.[21] Our approach in the present work is to adhere 100 nm thick Au SRRs to a 1 mm thick PDMS substrate. The metamaterial arrays are patterned on Si wafers using electron beam lithography. Electron beam evaporation is used to deposit 100 nm of Au, which is coated with a monolayer of 3-mercaptopropyl trimethoxysilane (MPT) under 50 mTorr vacuum. The MPT creates an Au–S bond at the surface that preferentially binds with the PDMS. Low-bias inductively coupled plasma reactive ion etching (ICP-RIE) with SF_6 is used to selectively remove the Si wafer leaving a freestanding 1 mm thick PDMS substrate with 100 nm thick metallic patterns on top.

Mechanical deformation of the substrate is used to stretch the resonators apart, changing both the capacitance of the SRR gap and the coupling strength between resonator pairs. Figure 1a,b shows metamaterial arrays on PDMS before and after stretching, respectively. The environmental scanning electron microscope (ESEM) image in Figure 1b shows the extent of deformation observed for a strain of $50 \pm 1\%$ in the y-direction. The strain is defined as $(l-l_0)/l_0 \times 100\%$, where l_0 is the initial length of the sample and the error is 1%. Different elements can be coupled to the SRR structure

to change the operating frequency. We examine four different samples (shown in Figure 1c with dimensions): SRR-bar, asymmetric coupled SRR (ACSRR), square SRR (sqSRR), and double SRR (DSRR) arrays.

Figure 2 shows the response of arrays of SRR-bar and ACSRR structures for strains of up to 50%. ESEM images of 4×4 arrays of unit cells are shown for the initial structures, the samples under 50% strain, and the samples after relaxation (Figure 2a,c). A custom-built stage is used to uniaxially stretch the compliant substrate. The coupling distance changes, as does the array period both parallel and perpendicular to the strain axis. The optical response of each sample was measured using Fourier Transform Infrared (FTIR) spectroscopy in reflection mode, and the spectra for the SRR-bar structures are shown in Figure 2b. We find that the observed resonance shifts are due to changes in coupling between the resonators and that the changing array period has a negligible effect. The spectrum has a reflection peak at 3.65 μm corresponding to the hybridized antisymmetric electromagnetic resonance of the unit cell.[21] Here we show the antisymmetric resonant mode of the array, although there is also a symmetric resonance, which is discussed in the Supporting Information. The sample was first strained 10% in the y-direction resulting in a blue shift of the resonant wavelength by 30 nm. The blue shift of the resonance frequency is due to the reduction in coupling strength when the coupled resonator elements are separated. The sample was then relaxed and the resulting data are coincident with the initial spectral position showing that for up to at least 10% strain the tuning is elastic in nature.

While elastic tunability of a metamaterial may be desirable, inelastic deformation could prove to be of particular importance for postfabrication tuning. For tensile strains of 20 and 50%, we observe the reflection peak shift by 80 and 140 nm, respectively. This corresponds to an initial SRR-bar distance of 50 nm and a stretched distance of 56 and 71 nm, as obtained from statistical analysis of ESEM images of arrays. After inducing a tensile strain of 50%, the elastomeric substrate was relaxed. The reflection peak position after relaxation is red shifted by 260 nm from the initial resonant peak, suggesting that the nanowire is closer to the resonator than in the original position. This is corroborated by the ESEM image (Figure 2a), which shows that the SRR-bar coupling distance is now 35 nm due to the permanent plastic deformation of the PDMS. Full-field electromagnetic simulations of the reflectance of the metamaterial arrays, calculated as described in ref 11, are shown in Figure 2b and these data agree well with the experimental results.

Changing the geometry of the resonant element from a nanowire to an asymmetric SRR reduces the resonant line width, improving tunability. Figure 2d shows the reflectance data for the array of ACSRRs. The initial reflection peak position is observed at 3.90 μm for a coupling distance of 60 nm. Elastic tuning was achievable up to 10% and, in this case, the peak was blue shifted 70 nm, double the wave-
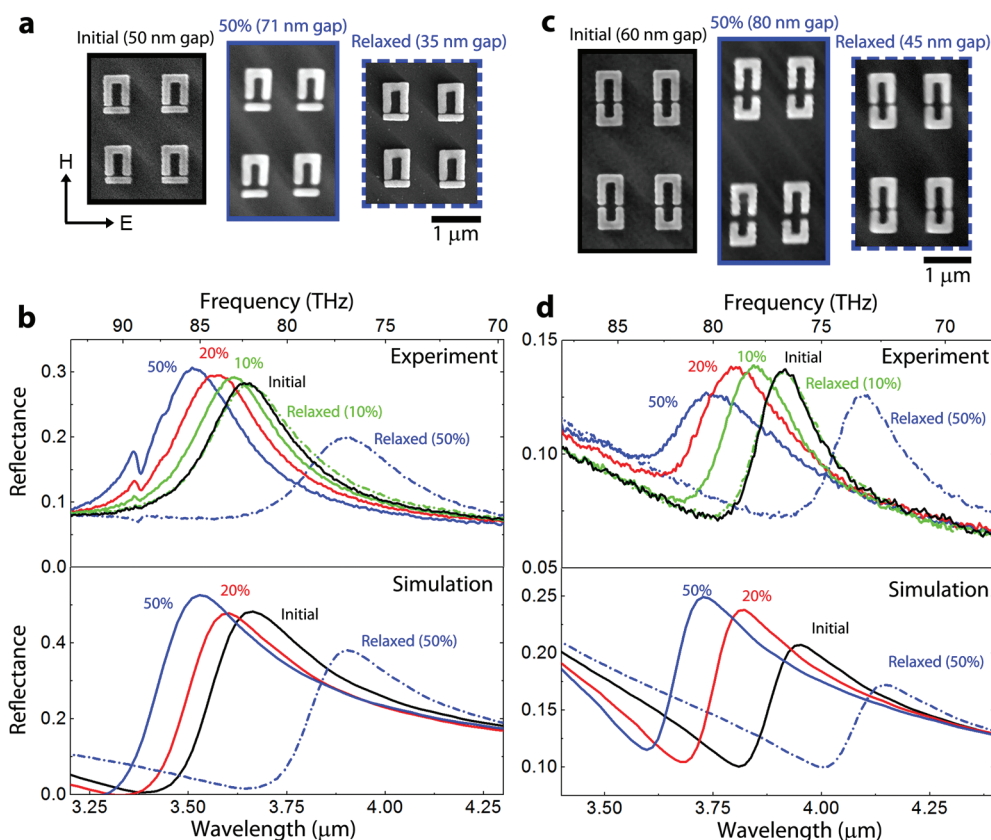
FIGURE 2. (a) ESEM images of an array of 2 × 2 SRR-bar unit cells initially, relaxed, and for 50% strain. The measured gap distances from ESEM images are shown in parentheses. (b) The experimental FTIR reflectance data for an array of SRR-bar structures under applied strains of up to 50% are shown in the top panel and the corresponding simulated reflectance data are shown in the bottom panel. (c) ESEM images of an array of 2 × 2 ACSRR unit cells initially, relaxed, and under 50% strain. The measured gap distances from ESEM images are shown in parentheses. d. The experimental FTIR reflectance data for an array of ACSRRs under applied strains of up to 50% are shown in the top panel and the corresponding simulated reflectance data are shown in the bottom panel.

length shift for the SRR-bar structure. For strains of 20 and 50%, the coupling distance is increased to 72 and 85 nm and the resonance is observed at 3.78 and 3.74 μm, respectively. After relaxing the sample, the SRRs are closer than in the original sample and the coupling distance was reduced to 45 nm, corresponding to a final resonance position of 4.07 μm. The simulation data for the ACSRR array are shown in the bottom panel of Figure 2d and agree well with the experiment.

Tunability ranges vary for the different arrays due to the sensitivity of the resonant wavelength shift on the coupling mechanism of the SRR designs. To compare the effect of strain on the tunability range for various resonator designs, we define a figure of merit (FOM) as the resonant wavelength shift, $\Delta\lambda$, divided by the full width at half-maximum (FWHM) of the initial reflection peak. The top panels of Figure 3a–d compare FOM as a function of mechanical strain. We induced tensile strains of up to 50% in the y-direction and 25% in the x-direction. Finite element modeling (FEM) results showing maps of normalized strain in the top layer of PDMS for each of the four SRR unit cells are displayed in the bottom panels with arrows indicating displacement vectors. For the sqSRR structure (Figure 3a), a maximum

FOM of 0.4 for 50% strain is measured. From the FEM simulations of strain, we see that stretching along the y-direction brings the arms closer, resulting in a decrease of the sqSRR gap. As a result, the effective capacitance increases, red shifting the resonant wavelength. The converse is true for stretching in the x-direction. With this simple sqSRR design, mechanical tuning can only affect the gap capacitance.

To increase the tunability range, more complex designs are necessary. We then explore coupled resonators, such as the DSRR[23] (Figure 3b), for which the FOM can be increased to almost 0.6. Plotting the FOM data shown in Figure 2 for the SRR-bar and the ACSRR structures, we note that increased coupling can indeed yield higher tunability. For the SRR-bar structure, we achieve a maximum FOM of 0.6 for strain applied along the y-direction and 0.4 for strain applied along the x-direction (Figure 3c). For the ACSRRs, we achieve line width tunability by stretching the array in either direction (Figure 3d). Coupled SRRs of differing size yield narrow electromagnetic resonances,[24] and thus the FOM is highest for the ACSRR configuration.

Mechanical modeling for the DSRR shows that as the structure is strained, the arms of the outer SRR bend inward,
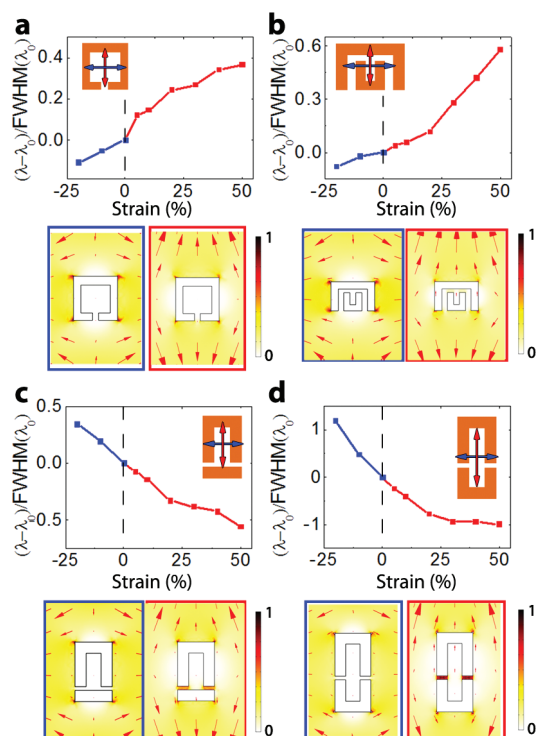
FIGURE 3. The top panel of each figure shows the reflection peak position shift divided by the FWHM of the initial reflection peak for the four different arrays stretched along the primary strain axis (positive tensile strain, shown in red) and the secondary strain axis (negative compressive strain, shown in blue), the square SRR data are shown in (a) the double SRR data are shown in (b) the SRR-bar data are shown in (c), and the asymmetric coupled SRR data are shown in (d). The bottom panel of each figure shows the strain density map for perturbations along the primary (red outline) or secondary (blue outline) strain axis. These data are normalized to the maximum for the SRR-bar configuration.

FIGURE 4. (a) The experimentally measured spectra for the DSRR structure array for tensile strains of up to 50%. ESEM images of structures initially, under various amounts of strain, and relaxed are shown. (b) Electric field intensity plots at the vibrational mode resonant wavelength (3.37 μm) for the initial structure and at 40% strain are shown. (c) The signal enhancement for the CH stretch vibrational mode as a function of observed tensile strain is shown.

increasing the coupling with the inner SRR and, in turn, the FOM. In the case of the SRR-bar and the ACSRR, however, the modeling shows that as the coupling element stretches away from the SRR, the highest region of strain is located in the gap and the displacement vectors show that these structures stretch uniaxially and do not experience bending as in the DSRR or sqSRR structures. This understanding of the nanomechanics provides useful insight for designing coupled resonators at the nanoscale for certain types of deformation and predicting the consequent mechanical and optical behavior.

Nanophotonic metallic structures, such as plasmonic resonators and metamaterials that enhance the electric fields at the near-field, find applications in spectroscopic techniques such as surface-enhanced infrared absorption (SEIRA)[25−27] and surface-enhanced Raman scattering (SERS)[28−30] for biological and chemical sensing.[31−33] Here, we exploit the mechanical tuning of the electromagnetic resonances of metasurfaces to amplify the signal of an infrared vibrational mode for surface enhanced reflection spectroscopy. In Figure 4a, the measured reflectance spectra and representative ESEM images for various degrees of strain are shown
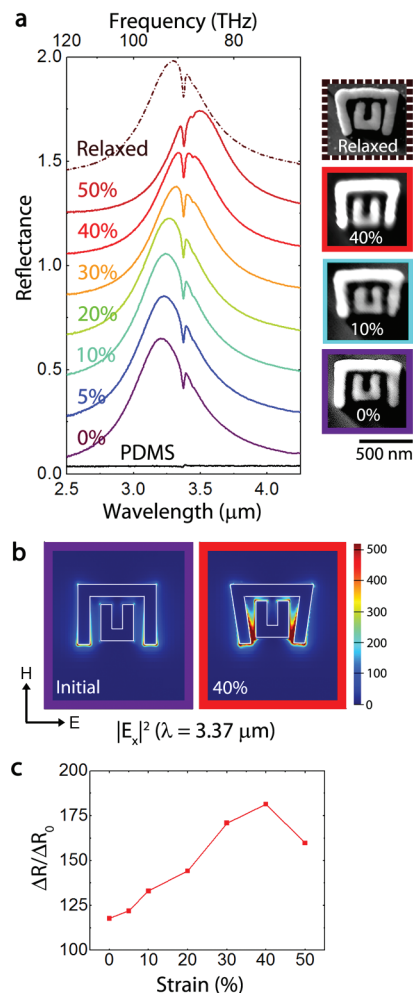
for the DSRR array. In the reflection spectra of a PDMS substrate without metallic nanostructures, we observe a weak absorption feature at 3.37 μm which corresponds to the vibrational mode of the C−H stretch bond.[34] Prior to stretching, the resonant wavelength of the metamaterial is 3.21 μm. We observe a reflection dip associated with the coupling of the metamaterial resonance to the C−H stretch vibrational mode.

By introducing mechanical strains up to 50%, we are able to controllably tune the resonant wavelength of the metamaterial through the C−H vibrational absorption at 3.37 μm. For 40% strain, we find that the peak of the metamaterial resonance is at 3.37 μm, coincident with the spectral position of the vibrational mode, resulting in increased absorption. Using full-field electromagnetic simulation, we calculate the total electric field intensities for the initial and 40% strained DSRR at 3.37 μm as shown in Figure 4b. Given that

the resonance of the initial DSRR is at a lower wavelength (3.22 μm), the electric field intensity at 3.37 μm is much lower than for the 40% strained DSRR. In Figure 4c, we report the enhancement factor for the signal, $\Delta R/\Delta R_0$, which is the ratio of the resonator-enhanced absorption to the absorption from bare PDMS. For a resonator array in un-strained PDMS the enhancement factor is 115, whereas at a strain of 40%, the absorption is enhanced by a factor of 180. We observe a 1.6-fold increase in the reflection signal upon optimizing the strain. The absorption enhancement is attributed to the electric field enhancement in "hot spot" regions between the two resonator legs and is maximized when the resonance of the metamaterial is matched to the C–H stretch vibrational mode as evident from the electric field intensity plots. The metallic nanostructures are on the surface of the substrate, thus we are only enhancing the reflection signal from the PDMS at the metal interfaces in the gap between resonator pairs. Given the in situ tuning capability of this type of structure, resonators could be designed to operate over a certain bandwidth and "focus" on peaks at particular frequencies. Mechanically deformable metamaterials could provide a more sensitive, broadband platform for both SEIRA and SERS measurements enabling sensing of low-concentration solutions of chemicals and biological agents.

We also extend the concept of mechanical tuning of electromagnetic resonances to plasmonic nanocavities. Recently, optical Fano resonances using coupled plasmonic nanostructures have received considerable interest.[17−20] Here, we study a dolmen-type resonator[18,20,35] and demonstrate how mechanical tuning can be used to modulate the Fano response. The dolmen-resonator consists of two plasmonic components: (i) a pair of metal strips with a dark-mode (subradiant) resonance and (ii) a monopole antenna exhibiting a bright-mode (super-radiant) resonance. Coupling these two resonant elements yields a Fano-type resonance. The experimental data for various strains are shown in Figure 5a. The initial spectrum has distinct resonances at 2.72 and 3.18 μm with a reflection dip at 2.95 μm. When the dolmen-resonator array is strained along the y-direction, the coupling distance, d_y, increases causing a decrease in the coupling strength similar to that observed for the SRR-bar geometry. For 20% strain, we observe that the λ_1 reflection peak blue shifts and the peak amplitude decreases with reduced coupling between the bright and dark modes. We then relax the sample to its original position and the second reflection peak reappears. We repeat the same procedure for 50% strain and note that the second reflection peak becomes almost imperceptible (red line). The dashed red line in Figure 5a shows the measured reflection spectra after relaxation, demonstrating that we are able to recover the Fano resonance after inducing a tensile strain. We observe that the reflection peak positions shift from the original positions due to plastic deformation upon stretching. This results in a decrease of d_y, leading to stronger coupling
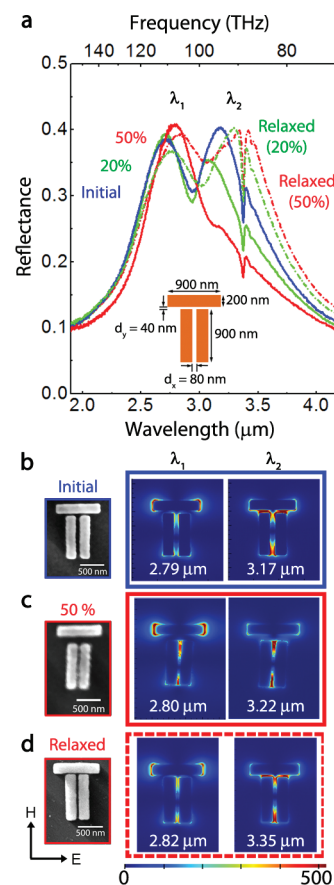

FIGURE 5. (a) The experimentally measured spectra of the Dolmen-resonator structure for observed strains of up to 50%. The schematic of the dolmen-resonator structure with dimensions is shown as an inset to the graph. (b) An ESEM image showing the unit cell initially and the electric field density at λ_1 and λ_2, the two reflection peak positions. (c) An ESEM image for the unit cell under 50% tensile strain and the corresponding electric field intensity plots at λ_1 and λ_2. (d) An ESEM image for the unit cell after relaxation and the corresponding electric field intensity plots at λ_1 and λ_2.

between resonators in a pair, and is evident in the ESEM image of the relaxed sample.

We use digitized ESEM images of characteristic unit cells to calculate the total electric field intensities using full-field electromagnetic simulation. In Figure 5b, we plot the electric field intensities for the two reflection peaks, λ_1 and λ_2, prior to stretching. The electric field is strongly enhanced at the tips of the optical monopole antenna at λ_1 due to the dipole antenna resonance. At λ_2, the electric field is strongly localized between the optical antenna and the wire pair as a result of strong coupling between these two resonant elements. In Figure 5c, we plot the field intensities for 50% strain at $\lambda_1 = 2.80$ μm (left) and $\lambda_2 = 3.22$ μm (right). The coupling distance (d_x) increases, but the distance between the metal wire pair (d_y) decreases, resulting in an enhanced field between the metal wire pair for both resonances. At λ_2 however, the fields are not strongly localized between the wire pair and the optical antenna due to reduced coupling. The field intensity of the relaxed structure (Figure 5d) is similar to the plot for the initial structure; however, the

reflection peak positions are shifted to $\lambda_1 = 2.82\ \mu$m and $\lambda_2 = 3.35\ \mu$m. We note that the λ_2 reflection peak is now aligned with the C−H vibrational mode and this signal is enhanced by a factor of almost 120.

We have demonstrated large strain mechanical deformation of a compliant metamaterial to achieve resonant frequency tuning by up to a line width and have exploited the mechanical control of coupled resonators to tunably enhance infrared absorption of a molecular vibrational mode, which could provide a new degree of freedom in molecular sensing and detection. We expect that the structures reported here are the first of a new class of highly compliant bendable, stretchable and tunable metamaterials, signaling a departure from the use of brittle, hard inorganic materials to achieve complex optical material responses.

Supporting Information Available. Symmetric versus antisymmetric modes of asymmetric coupled systems. This material is available free of charge via the Internet at http://pubs.acs.org.

REFERENCES AND NOTES

(1) Shalaev, V. M. *Nat. Photonics* **2007**, *1*, 41–48.
(2) Smith, D. R.; Pendry, J. B.; Wiltshire, M. C. K. *Science* **2004**, *305*, 788–792.
(3) Rogacheva, A. V.; Fedotov, V. A.; Schwanecke, A. S.; Zheludev, N. I. *Phys. Rev. Lett.* **2006**, *97*, 177401.
(4) Gansel, J. K.; Thiel, M.; Rill, M. S.; Decker, M.; Bade, K.; Saile, V.; von Freymann, G.; Linden, S.; Wegener, M. *Science* **2009**, *325*, 1513–1515.
(5) Chen, H.-T.; Padilla, W. J.; Zide, J. M. O.; Gossard, A. C.; Taylor, A. J.; Averitt, R. D. *Nature* **2006**, *444*, 597–600.
(6) Tao, H.; Strikwerda, A. C.; Fan, K.; Padilla, W. J.; Zhang, X.; Averitt, R. D. *Phys. Rev. Lett.* **2009**, *103*, 147401.
(7) Dicken, M. J.; Aydin, K.; Pryce, I. M.; Sweatlock, L. A.; Boyd, E. M.; Walavalkar, S.; Ma, J.; Atwater, H. A. *Opt. Express* **2009**, *17*, 18330–18339.
(8) Samson, Z. L.; MacDonald, K. F.; De Angelis, F.; Gholipour, B.; Knight, K.; Huang, C. C.; Di Fabrizio, E.; Hewak, D. W.; Zheludev, N. I. *Appl. Phys. Lett.* **2010**, *96*, 143105.
(9) Xiao, S. M.; Chettiar, U. K.; Kildishev, A. V.; Drachev, V.; Khoo, I. C.; Shalaev, V. M. *Appl. Phys. Lett.* **2009**, *95*, No. 033114.
(10) Chen, H. T.; O'Hara, J. F.; Azad, A. K.; Taylor, A. J.; Averitt, R. D.; Shrekenhamer, D. B.; Padilla, W. J. *Nat. Photonics* **2008**, *2*, 295–298.
(11) Rogers, J. A.; Someya, T.; Huang, Y. G. *Science* **2010**, *327*, 1603–1607.
(12) Huang, F.; Baumberg, J. J. *Nano Lett.* **2010**, *10*, 1787–1792.
(13) Olcum, S.; Kocabas, A.; Ertas, G.; Atalar, A.; Aydinli, A. *Opt. Express* **2009**, *17*, 8542–8547.
(14) Melik, R.; Unal, E.; Perkgoz, N. K.; Puttlitz, C.; Demir, H. V. *Appl. Phys. Lett.* **2009**, *95*, 3.
(15) Tao, H.; Bingham, C. M.; Strikwerda, A. C.; Pilon, D.; Shrekenhamer, D.; Landy, N. I.; Fan, K.; Zhang, X.; Padilla, W. J.; Averitt, R. D. *Phys. Rev. B* **2008**, *78*.
(16) Tao, H.; Strikwerda, A. C.; Fan, K.; Bingham, C. M.; Padilla, W. J.; Zhang, X.; Averitt, R. D. *J. Phys. D: Appl. Phys.* **2008**, *41*, 5.
(17) Fan, J. A.; Wu, C. H.; Bao, K.; Bao, J. M.; Bardhan, R.; Halas, N. J.; Manoharan, V. N.; Nordlander, P.; Shvets, G.; Capasso, F. *Science* **2010**, *328*, 1135–1138.
(18) Verellen, N.; Sonnefraud, Y.; Sobhani, H.; Hao, F.; Moshchalkov, V. V.; Van Dorpe, P.; Nordlander, P.; Maier, S. A. *Nano Lett.* **2009**, *9*, 1663–1667.
(19) Sonnefraud, Y.; Verellen, N.; Sobhani, H.; Vandenbosch, G. A. E.; Moshchalkov, V. V.; Van Dorpe, P.; Nordlander, P.; Maier, S. A. *ACS Nano* **2010**, *4*, 1664–1670.
(20) Zhang, S.; Genov, D. A.; Wang, Y.; Liu, M.; Zhang, X. *Phys. Rev. Lett.* **2008**, *101*, No. 047401.
(21) Aydin, K.; Pryce, I. M.; Atwater, H. A. *Opt. Express* **2010**, *18*, 13407–13417.
(22) Sersic, I.; Frimmer, M.; Verhagen, E.; Koenderink, A. F. *Phys. Rev. Lett.* **2009**, *103*, 213902.
(23) Liu, N.; Guo, H. C.; Fu, L. W.; Schweizer, H.; Kaiser, S.; Giessen, H. *Phys. Status Solidi B* **2007**, *244*, 1251–1255.
(24) Fedotov, V. A.; Rose, M.; Prosvirnin, S. L.; Papasimakis, N.; Zheludev, N. I. *Phys. Rev. Lett.* **2007**, *99*, 147401.
(25) Bukasov, R.; Shumaker-Parry, J. S. *Anal. Chem.* **2009**, *81*, 4531–4535.
(26) Jensen, T. R.; Van Duyne, R. P.; Johnson, S. A.; Maroni, V. A. *Appl. Spectrosc.* **2000**, *54*, 371–377.
(27) Kundu, J.; Le, F.; Nordlander, P.; Halas, N. J. *Chem. Phys. Lett.* **2008**, *452*, 115–119.
(28) Le, F.; Brandl, D. W.; Urzhumov, Y. A.; Wang, H.; Kundu, J.; Halas, N. J.; Aizpurua, J.; Nordlander, P. *ACS Nano* **2008**, *2*, 707–718.
(29) Wang, H.; Kundu, J.; Halas, N. J. *Angew. Chem., Int. Ed.* **2007**, *46*, 9040–9044.
(30) Lal, S.; Grady, N. K.; Kundu, J.; Levin, C. S.; Lassiter, J. B.; Halas, N. J. *Chem. Soc. Rev.* **2008**, *37*, 898–911.
(31) Cubukcu, E.; Zhang, S.; Park, Y. S.; Bartal, G.; Zhang, X. *Appl. Phys. Lett.* **2009**, *95*, No. 043113.
(32) Neubrech, F.; Pucci, A.; Cornelius, T. W.; Karim, S.; Garcia-Etxarri, A.; Aizpurua, J. *Phys. Rev. Lett.* **2008**, *101*, 157403.
(33) Liu, N.; Weiss, T.; Mesch, M.; Langguth, L.; Eigenthaler, U.; Hirscher, M.; Sonnichsen, C.; Giessen, H. *Nano Lett.* **2010**, *10*, 1103–1107.
(34) Smith, A. L.; Anderson, D. R. *Appl. Spectrosc.* **1984**, *38*, 822–834.
(35) Liu, N.; Langguth, L.; Weiss, T.; Kastel, J.; Fleischhauer, M.; Pfau, T.; Giessen, H. *Nat. Mater.* **2009**, *8*, 758–762.